DESIGN OF RECONFIGURABLE INTELLIGENT SURFACE FOR 5G WIRELESS COMMUNICATION SYSTEM

BY

YUJIANG HAN

THESIS

Submitted in partial fulfillment of the requirements
for the degree of Master of Science in Electrical and Computer Engineering
in the Graduate College of the
University of Illinois Urbana-Champaign, 2024

Urbana, Illinois

Adviser:

Associate Professor Zhen Peng

Abstract

Wireless communication systems have seen remarkable advancements in recent years, driven by the ever-growing demand for high-speed, reliable connectivity. Reconfigurable Intelligent Surfaces (RISs) have emerged as a promising technology to address the challenges of wireless communication, offering unprecedented control over electromagnetic wave propagation in various environments. In addition, RISs can be fabricated with low cost and can be controlled easily by the user. Meanwhile, RIS has wide adaption to the optimization algorithm, low power consumption. With all the advantages RISs can provide, it has been considered as one potential area that could lead the wireless communication into next era. This thesis develops one type of RIS based on the prototype design from Arizona State University [1]. A two state, 25 elements RIS, has operating frequency at 5.8 GHz, is designed and simulated by using full-wave simulator. The unit cell of the prototype design can be controlled by using a RF switch, which can switch between two states, [0, 180], to change the reflectivity of the surface to apply a 180-degree phase shift for the wave. Since nowadays the wireless communication systems for public use (Wi-Fi, cell phone network, and etc.) has operating frequency at 5 – 5.8 GHz, the prototype designed is capable to use to enhance the performance for those systems. Moreover, the prototype design can be fabricated and implemented on PCB board, which further minimizes the difficulties and cost for the implementation of the RIS.

Acknowledgments

I would like to express my sincere gratitude to Professor Zhen Peng for his invaluable guidance, support, and mentorship throughout the course of my thesis. His expertise and insightful feedback have greatly enriched this work.

I am also grateful to Qi Jian and Charles for their assistance, collaboration, and contributions to various aspects of this research project. Their dedication and expertise have been instrumental in the successful completion of this thesis. Additionally, I extend my thanks to all my colleagues and friends who provided support and encouragement during this endeavor.

Contents

1. Introduction

In the era of ubiquitous connectivity and escalating demands for high-speed wireless communication, the quest for innovative solutions to enhance spectral efficiency and coverage has become paramount. The exponential growth in wireless data traffic, driven by the proliferation of mobile devices, Internet of Things (IoT) applications, and bandwidth-intensive multimedia services, has imposed unprecedented challenges on existing wireless communication infrastructure. Traditional approaches relying solely on macrocellular networks and base station densification are reaching their limits in meeting the ever-increasing demand for connectivity. As a result, there is a pressing need for disruptive technologies capable of unlocking untapped spectral resources, enhancing coverage, and improving energy efficiency. Reconfigurable Intelligent Surfaces offer a compelling solution to these challenges by leveraging programmable Meta Surfaces to manipulate electromagnetic waves dynamically. By strategically adjusting the phase and amplitude of reflected signals, RIS can shape propagation environments, mitigate interference [2], and enhance signal strength [3], thereby enabling significant performance gains in wireless communication systems. With all the potentials, it is beneficial to test the RIS in modern wireless communication systems. With this motivation, this thesis designs a portable, low cost, low power binary RIS for modern wireless communication systems.

1.1 Background

Wireless communication engineers aspire to realize a seamlessly connected world, where wireless connectivity is ubiquitous for all entities. With the wide application of current 5G networks and the impending arrival of 6G, there arises an unprecedented demand for connectivity at an unparalleled scale. Meeting this demand necessitates future wireless networks to be smart, intelligent, and efficient. Traditionally, the dynamic and adaptive features of mobile networks have been controlled solely by the base station or user equipment, with the wireless propagation environment remaining oblivious to the communication processes traversing through it. However, existing mobile network operators face the

formidable challenge of ensuring seamless connectivity in challenging propagation environments while accommodating an ever-growing number of mobile users, often distributed unevenly across the network. While large-scale antenna systems can partially address these challenges, obstructions in complex environments like buildings, trees, tunnels, glasses, and multipath interferences can severely affect transmission and communication quality in certain areas. Relay nodes, commonly employed to mitigate such issues, often result in increased power consumption and undesirable effects on signal-to-noise ratio [4]. Extensive research has been conducted to tackle these challenges. However, there remains an ongoing discourse in both industrial and academic circles regarding the design and evaluation of technologies capable of imbuing intelligence into the otherwise passive radio propagation environment. Reconfigurable Intelligent Surface (RIS) has adjustable reflective unit cell patches to attenuate the phase and amplitude of the reflected wave. By adjusting the tunable reflective unit cell, phase and amplitude can be manually modulated, and therefore, we can change the reflective angle, redirecting the beam to targeted directions.

When a wave packet interacts with an interface, it typically reflects according to Snell's law of reflection on the plane of incidence, maintaining a constant relative angle between the normal vector to the reflecting interface and the incident wave vector (θi), resulting in $\theta i = \theta r$, where θr denotes the angle of the reflected rays. However, Reconfigurable Intelligent Surfaces (RIS) offer a unique capability to deviate from this phenomenon, allowing for the inclination of reflecting waves towards a desired direction, thus breaking the convention where θi is not necessarily equal to θr. This concept, known as engineered reflection or anomalous reflection, requires the reflection phase to be linearly dependent on the corresponding coordinate along the surface interface, a condition satisfied by principles such as the 'generalized Snell's law' or the 'holographic technique' [4]. Let us imagine that a wave incidence on a relatively large surface with incident angle θi, and the surface has impedance η_s. The reflection coefficient can be formulated as:

$$\Gamma = \frac{\eta_s - \eta_0}{\eta_s + \eta_0}. \tag{1.1}$$

Since RIS has tunable surface impedance, by changing the surface impedance η_s, users can change the reflection coefficient of the surface and direct the reflected wave to desired direction.

For the RIS design, a switch positioned at the feed of a resonant metallic patch has the capacity to alter the pathway of electric current, consequently influencing the amplitude and phase of the re-radiated field. Integration of multiple switches facilitates multi-bit wavefront modulation, thereby enhancing beam control and operational efficiency. Various configurations are documented in literature employing single or multiple active components and employing single or multi-layered substrates. In all configurations, a biasing circuit and control unit are essential components within the Reconfigurable Intelligent Surface (RIS) to regulate the state of tunable devices by adjusting the biasing voltage. RIS structures are typically considered two-dimensional due to lateral dimensions spanning multiple wavelengths, with thickness typically being only a fraction of a wavelength. These geometric characteristics facilitate seamless installation on building surfaces, encompassing curved surfaces, both indoors and outdoors [1].

1.2 OFDM Wireless Communication System with RIS

The Reconfigurable Intelligent Surface (RIS) operates by scattering or reflecting the incident wave according to its configuration. In scenarios featuring a single-antenna transmitter and single-antenna receiver, communication performance hinges on the Signal-to-Noise Ratio (SNR). Consequently, the RIS can enhance system performance by optimizing its reflection coefficients to maximize received signal power. This entails ensuring that the individually reflected signals from RIS elements reach the receiver in phase, albeit limited by hardware granularity. When there exists a Line of Sight (LoS) channel from the RIS to the receiver, optimization efforts essentially result in a reflected beam directed towards the receiver's angular position [5].

Orthogonal Frequency Division Multiplexing (OFDM) stands as one of the most prevalent schemes within wireless communities, finding extensive application in Wi-Fi and LTE communications. This modulation technique operates on the principle of multicarrier transmission, dividing the available bandwidth into numerous sub-carriers. Each channel corresponding to these sub-carriers is designed to be orthogonal to one another, ensuring minimal interference even when closely spaced. Additionally, the subdivision of bandwidth into smaller sub-carriers serves to mitigate the effects of channel fading, resulting in increased stability for each sub-carrier channel compared to wider bandwidths. With all these properties and extensive applications of OFDM, it is suitable to integrate the RIS with OFDM communication systems to enhance the quality of the communication.

Normal communication system usually transmits data in time domain, however OFDM can divide the bandwidth into small sub-carriers and transmit the data in frequency domain. When OFDM symbols were being transmitted in the channel, we can use mathematical equations to model the entire process:

$$y[n] = h[n] \otimes x[n] \tag{1.2}$$

$$Y[k] = H[k]X[k] \tag{1.3}$$

$$\mathrm{IDFT: x}[n] = \frac{1}{N}\sum_{k=0}^{N-1} \mathrm{X}[k]e^{j\frac{2\pi kn}{N}} \tag{1.4}$$

$$\mathrm{DFT: X[k]} = \sum_{n=0}^{N-1} \mathrm{x}[n]e^{-j\frac{2\pi kn}{N}} \tag{1.5}$$

In our analysis, we examine a basic situation where the interaction between a single-antenna transmitter and a single-antenna receiver is supported by a RIS. We assume this surface possesses a consistent flat array arrangement comprising M×N unit cells. Utilizing an OFDM (Orthogonal Frequency Division Multiplexed) system framework comprising K sub-carriers, we establish $h_{TX,k}$ and $h_{RX,k}$ as the MN × 1 uplink channels from the transmitter and receiver to the RIS, respectively, with k ranging from 1 to K.

Additionally, we define $h_{TR,k}$ as the direct Line of Sight (LoS) channel between the transmitter and receiver on the k-th subcarrier. If s_k represents the transmitted signal over the k-th subcarrier, the received signal can be expressed as follows [1]:

$$r_k = h_{RX,k}^T \Psi h_{TX,ks_k} + h_{TR,ks_k} + n_k. \quad (1.6)$$

Where n_k is used to represent the noise and ψ is for the *MN × MN* RIS interaction matrix. Ψ can include the phase control vector for each unit cell if we define a diag(Ψ) as *MN × 1* RIS reflection vector. Then the phase control vector can be chosen by the users to maximize the received power on the receiver side [1]. In our research, a QPSK (Quadrature Phase Shift Keying) OFDM System is developed by using GNURadio and USRP X310, the system can be used to transmit data like images and text messages at frequency 5.8 GHz. Please see the Appendix A for more about GNURadio OFDM system information.

2. Literature Review

RIS has attracted significant attention from both antenna and communication academic and industry. During recent years, there are numerous prototypes and research emerging in this area, discussing the design and control optimization for RIS [21]. With the potential that RIS has to accelerate the communication development and the innovative properties, RIS draws my interest immediately. Before I started my Master program, I was already interested in hardware design and digital communication. RIS could be a great learning chance for me to improve and combine hardware design, EM wave theory, and digital communication skills. With the motivation behinds it, this thesis mainly develops and simulates a low cost, low power consumption, simple structure RIS which has operation frequency at 5.8 GHz, a frequency band commonly used on Wi-Fi and LTE, by referring mainly to the prototype and RIS design in papers "Design and Evaluation of Reconfigurable Intelligent Surfaces in Real-World Environment" [1] and "Reconfigurable Intelligent Surface (RIS) in the Sub-6 GHz Band: Design, Implementation, and Real-World Demonstration"[4].

In this thesis, we are introducing a single-layer, single switch-per-cell design for Reconfigurable Intelligent Surfaces (RIS), operational at 5.8 GHz and compatible with mmWave and THz fabrication and integration technologies. This layout eliminates the need for vertical connections (e.g., vias) and incorporates the biasing network on the same plane [1]. Prototype can be fabricated on PCB, integrating with PIN diodes, which are used as RF switches to control the phase modulation. The prototype also has the beamforming abilities in outdoor environments when interacting with base transmitter and receiver (e.g., USRPs).

3. RIS Unit Cell Design

In this chapter, we will introduce the design of RIS unit cell in detail, with the unit cell layout design, control unit design, and control unit testing board design. The RIS is crafted to function at a central frequency of 5.8 GHz, aligning with the unlicensed spectrum utilized in wireless local area networks (WLANs). This endeavor aims to devise a single-layer topology (excluding the ground plane) without necessitating the use of vias. Consequently, the RIS comprises the ground plane, the substrate, and the top metal layer. Such a configuration holds promise for forthcoming mmWave and THz RISs, as multilayer structures tend to elevate losses and fabrication intricacy [1].

3.1 RIS Unit Cell Layout

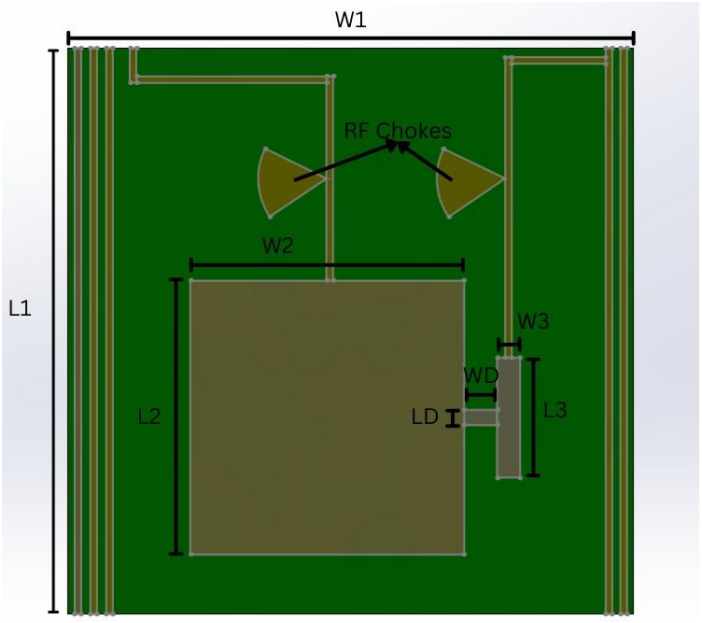

Figure 1. RIS Unit Cell Model

Parameters	Length (mm)
W1	25.85
L1	25.85
W2	12.51
L2	12.51
W3	1.75
L3	5.48
WD	1.5
LD	0.7

Table 1. RIS Unit Cell Model Parameters

The Reconfigurable Intelligent Surface (RIS) consists of 25-unit cells, organized in a 5 x 5 configuration. Each unit cell is consisted by a main resonant reflective metallic patch, a parasitic resonant metallic patch, a RF PIN diode, and traces, as shown in Figure 1. The unit cell is a square with width and length that is approximately half of the signal wavelength. Even though smaller the unit cell (e.g. $\lambda/4$ for unit cell width) is, better the control accuracy and flexibility users could have, the cost for fabrication and control optimization difficulties will increase since more unit cells are included and the size of the unit cell vector matrix will be larger. Therefore, to minimize the fabrication cost and lower the complexity of control of the RIS while having reasonable function and performance, half wavelength unit cell is implemented in the thesis.

The resonant patch re-radiates the received signal with a phase difference dependent on the current distribution, determined by the voltage applied across the diode terminals (reverse bias: OFF, forward bias: ON). Typically, this phase shift is achieved by altering the resonant frequency of the patch or providing additional path to the current on the feed of the patch [1] [4]. However, the second approach usually needs extra traces to the ground, which will include the via in the design. Vias could affect the electromagnetic (EM) characteristics of the entire RIS unit cell, the quality of the RF/EM signals, and increase the difficulties for fabrication. Therefore, we choose to add another parasitic resonant metallic patch and connect it to the main resonant patch by using PIN diode, so that we could prevent using vias in the RIS unit cell design to improve the beamforming performance and minimize the loss of the signal reflected by the RIS unit cell. The PIN diode (located at the position of WD and LD) mainly act like a switch for the incoming radio frequency (RF) signal, which connects the main metallic patch and parasitic patch. When the PIN diode is in forward bias (ON) mode, the current can flow from main patch to the parasitic patch, and by activating the parasitic patch, we change the characteristic surface impedance of the reflective patch and its resonant frequency, therefore a phase modulation will be applied to the signal without having significant attenuation on the signal magnitude.

In order for us to control the operating mode of PIN diode, a DC voltage must be applied on both sides of the diode. In the prototype design, both resonant patches are also utilized as the DC voltage biasing port for the PIN diode, and therefore, each patch is connected to a biasing trace to obtain DC voltage for PIN diode control. DC voltage on the biasing traces and patches will cause interference to the RF signal, which could attenuate the magnitude of the RF signal. To mitigate RF signal interference from the biasing lines, a radial RF choke is implemented within each line, adding some inductance above the resonant patches to isolate the interference from biasing DC voltage [6]. These biasing lines are organized in clusters of five unit cells to streamline wiring complexity, as depicted in the complete array topology illustrated in Fig. 1. In contrast to existing methodologies in literature, the proposed configuration necessitates only a solitary PIN diode and adopts a single-layer design devoid of vertical connections to the ground. While single-switch methods may produce quantization sidelobes, this study confines RIS usage to a restricted scanning range to circumvent sidelobe interference [1].

The RIS unit cell prototype design in here can be fabricated and printed on PCB board. The substrate used in the design is Rogers RT/Duroid 6002 RF laminate with thickness 2.54mm. The RT/Duroid 6002 laminate exhibits low dielectric loss, making it suitable for high-frequency RF and microwave applications. This characteristic helps minimize signal attenuation and distortion, ensuring efficient signal transmission. The laminate maintains stable electrical properties over a wide range of frequencies and temperatures. This stability is crucial for maintaining signal integrity and reliability in demanding RF and microwave circuits. RT/Duroid 6002 laminate is compatible with standard PCB fabrication processes, including drilling, routing, and soldering. Its ease of fabrication streamlines manufacturing processes and reduces production costs. Rogers RT/Duroid 6002 RF laminate has dielectric constant of 2.94 and loss tangent 0.0012, the parameters make the RT 6002 suitable for RF design. The PIN diode we used here is BAR50-02V, manufactured by Infineon and commonly used as RF

switch since it has great performance for high frequency RF signal and low internal resistance in forward bias mode.

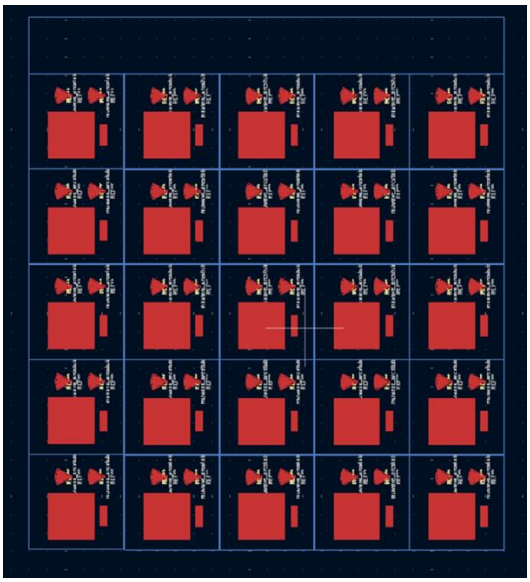

Figure 2. Layout of entire 25 unit cells RIS design (with hided biasing lines and diodes to make it clear)

3.2 RIS Control Unit Design

The main control unit we used for this prototype is Arduino MEGA 2560, which can provide multiple 5V digital/analog I/O ports for digital control signals and be easily programmed by the user. We will split the 25 unit cells into four groups of eight (one extra will be on its own), each group is connected to an 8-bit shift register. Both the register clock (RCK) and shift register clock (SRCK) signals from the control unit are distributed to all shift registers in parallel to ensure synchronization. The 8 bits on each output pin of the shift register are input serially and synchronized by the RCK signal. Subsequently, the outputs of all shift registers are simultaneously activated using the SRCK signal. Four 8-bit segment digital codes will be generated from Arduino for shift register, each bit represents the state of RIS unit cell (0 for OFF, 1 for ON). When the control bit for the unit cell is 1, a 0.8V voltage will be applied on the PIN diode, force the diode to enter forward bias mode, and enable the phase modulation for the reflected signal. Every output of the shift registers is connected to a resistor to have the voltage across the PIN diode to be

0.8V and limit the current to 3mA. Moreover, each PIN diode is connected to a LED indicator for debugging purpose (to indicate whether the PIN diode is ON or OFF). For reverse bias mode, the output voltage of shift register is 0V, therefore the PIN diode will not be turned on. The time required to update the state of the unit cell will depend on the internal clock frequency of main control Arduino [1]:

$$t_{update} = \frac{n_p \ N_s}{f_{clk}} \tag{3.1}$$

n_p is the number of bits of shift register (8 bit), N_s is the number of shift register in series ($N_s = 1$), and f_{clk} is the frequency of the internal clock (f_{clk} = 16MHz).

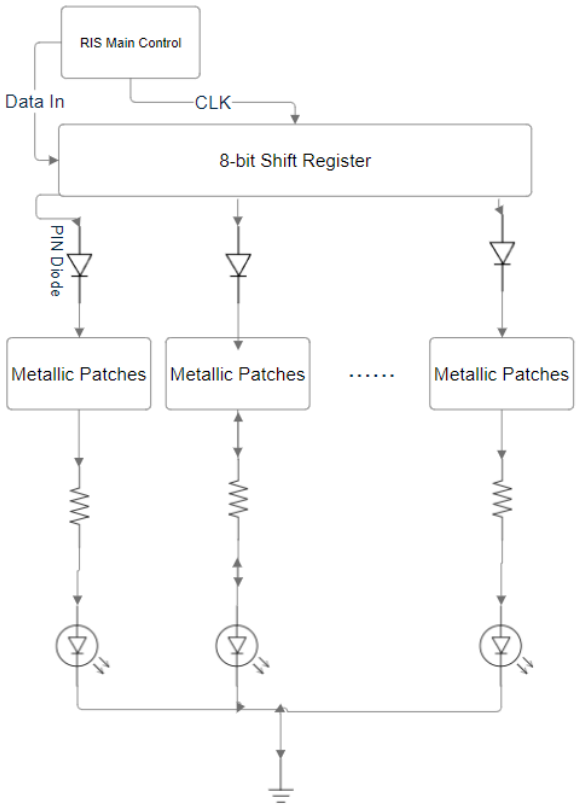

Figure 3. Control Unit Top-level Design

For control circuit testing and current limit resistor choosing, a testing unit cell is designed before we implement the actual control unit.

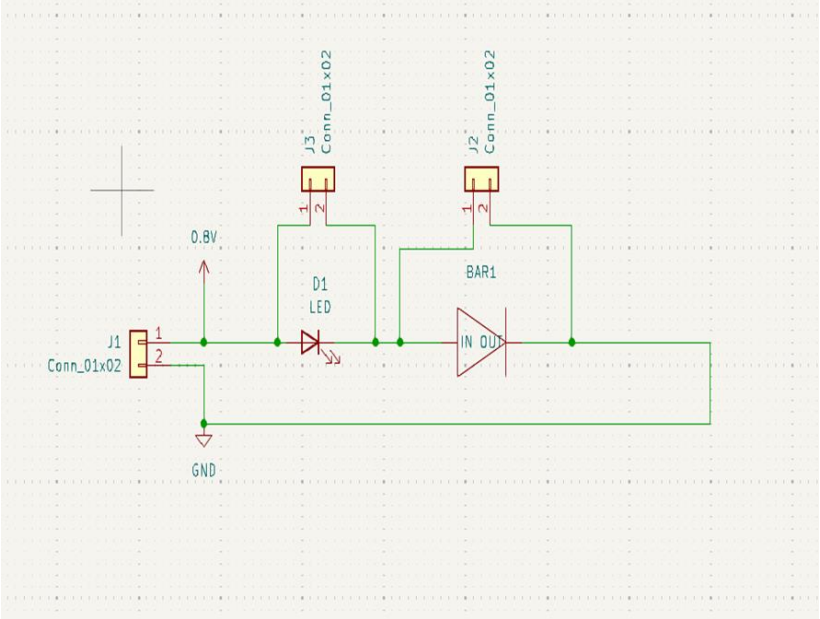

Figure 4. Testing unit cell schematics

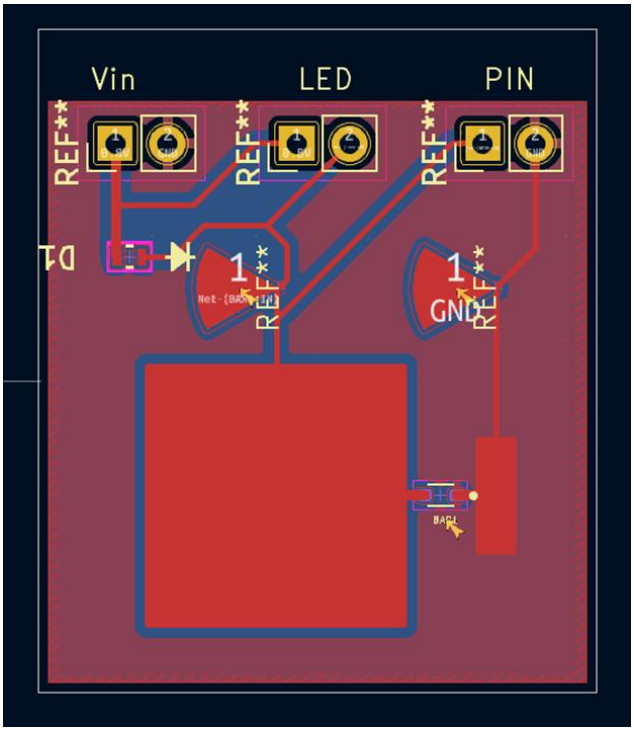

Figure 5. Testing unit cell layout

Reflective resonant patches are included with the radial RF chokes. The LED used in the design is SML-D12U8WT86, which has 1.2 – 1.9V working voltage for 3mA biasing current when it is being turned on.

The output voltage for shift register is 5V, which is the same as the voltage of Arduino output. A constant 5V DC source will be used to simulate the condition when a RIS unit cell is being turned on, connecting with a 1K Ohms potentiometer, and then feeding in to the Vin port on the testing unit cell. By tuning the potentiometer and monitoring the voltage across LED and PIN diode through the connector, we can limit the voltage across the PIN diode to be 0.8V and current to be 3mA, which will force the diode to enter forward bias mode and light the LED. By measuring the resistance of the potentiometer, we can find the resistor that works best with the unit cell circuit. In our design, the resistor used for limiting the current is 770 Ohms.

4. Simulation Result

To evaluate and measure the performance and functionality of the RIS unit cell in different states (forward bias and reverse bias), we used HFSS, an industry commercial full-wave simulator to simulate the response of the unit cell. A 3D unit cell model first was constructed by using SOLIDWORKS, a commercial 3D modeling CAD software, as depicted in Figure 6, then we extracted the geometry file from SOLIDWORKS and imported the 3D model into HFSS.

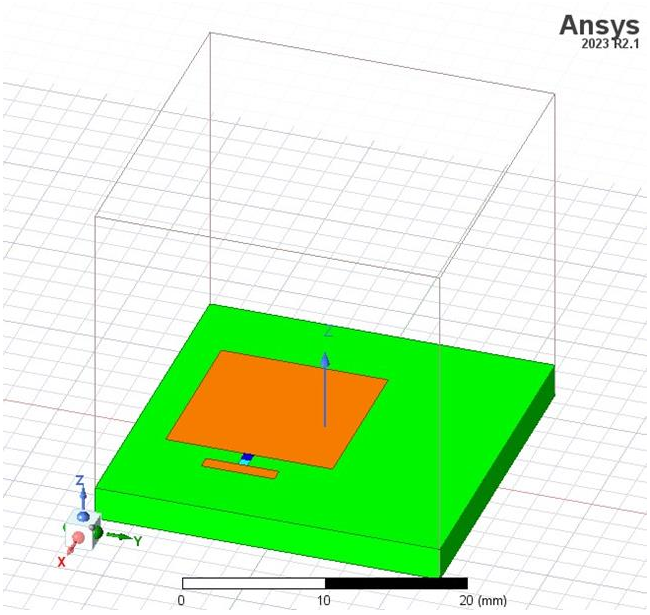

Figure 6. RIS unit cell 3D geometry model

The substrate employed in this model is the Rogers RT/Duroid 6002 RF laminate (RT 6002), same as the substrate in our design, featuring a dielectric constant, height, and loss tangent of 2.94, 2.54 mm, and 0.0012, respectively. Patches are printed by using PCB copper microstrip on the front side of the substrate, layered as a surface on RT 6002. PIN diode is being modeled by using equivalent circuit for different modes.

Figure 7. Reverse mode PIN diode equivalent circuit

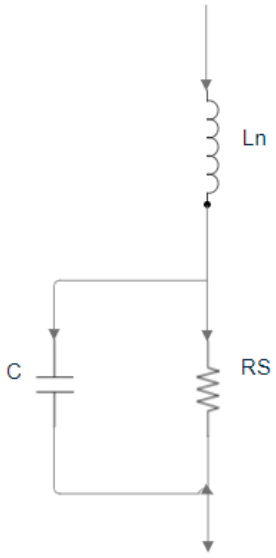

Figure 8. Forward mode PIN diode equivalent circuit

PIN diode can be modeled by using inductor (L_n), resistor (R_S), and Capacitor (C). PIN diode manufacturer Infineon provides the value of the components in equivalent circuit model.

For reverse bias mode, L_n = 0.6nH, R_S = 5000Ohms.

For forward bias mode, L_n = 0.6nH, R_S = 3Ohms, C = 0.15pF (For 0.8V, 3mA).

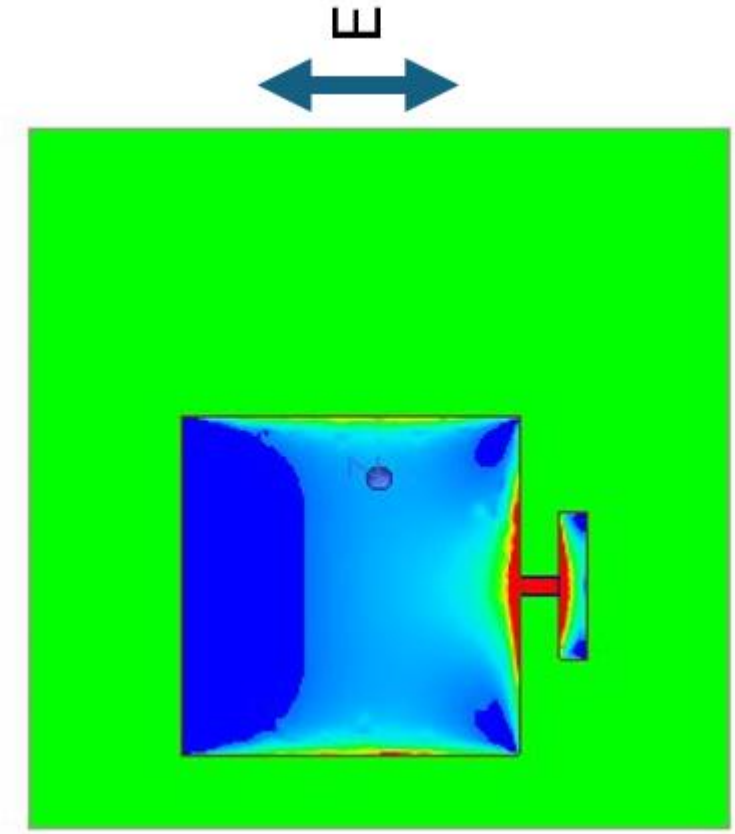

Figure 9. Horizontal E polarization with no biasing lines simulation

We first simulate the substrate with only the resonant reflective patches in HFSS, to verify the basic functionality of the reflective patch in different modes. Also, by adjusting the size of the parasitic resonant patch, a desired 180 degree phase modulation can be achieved at 5.8GHz in forward bias mode.

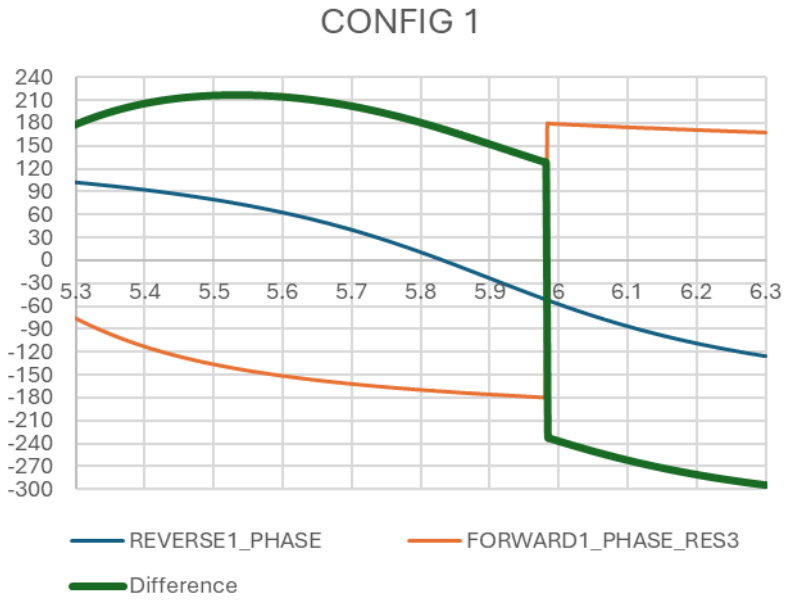

Figure 10. Phase modulation for reverse and forward bias modes, the green line indicates the phase difference between forward and reverse modes

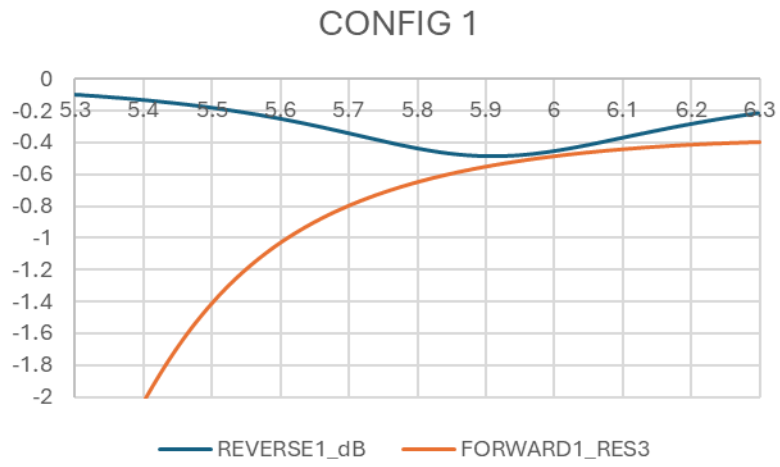

Figure 11. Magnitude attenuation (loss) for reverse and forward bias modes

The simulation results are shown in Figure 10 and 11. As depicted in the result, with just the reflective patches, we swept the frequency from 5.3GHz to 6.3GHz, at 5.8GHz, 180 degree phase shift difference can be achieved between forward and reverse bias mode, a 180 degree phase modulation has been applied to the signal. Moreover, both magnitude loss for reverse and forward modes are less than -1 dB at 5.8GHz, which is an acceptable range for signal attenuation and loss.

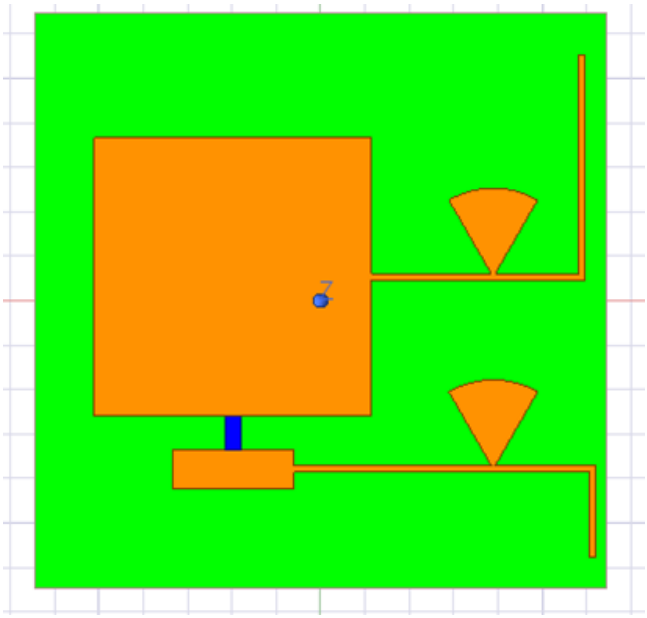

Figure 12. Simulation with radial RF chokes and biasing lines

After the size of parasitic resonant patch is fixed, radial RF chokes and biasing lines are added into the model and into consideration. The radius of the RF choke plays a significant role inside the simulation, and different radius sizing will affect the unit cell's performance in crucial ways.

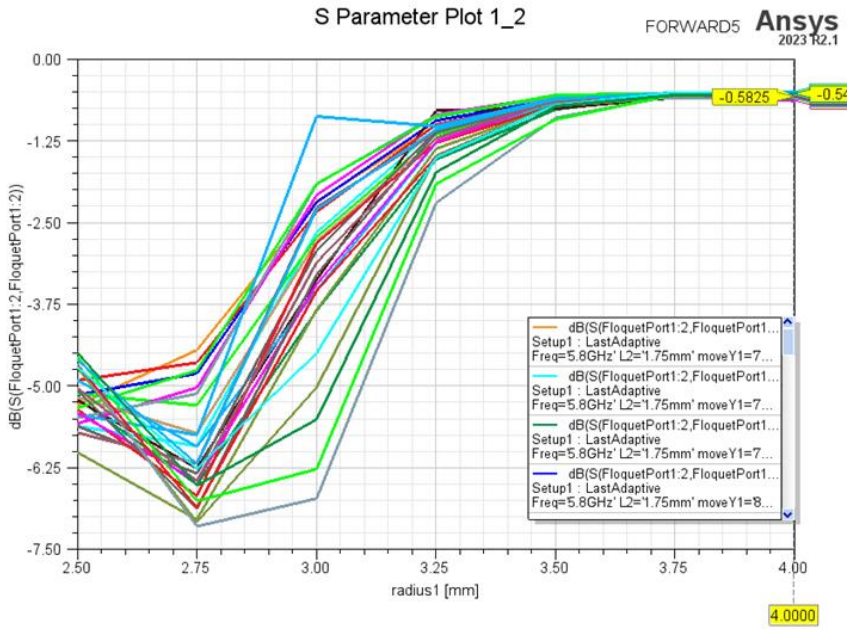

Figure 13. Magnitude attenuation (loss) for forward bias with different RF chokes radius

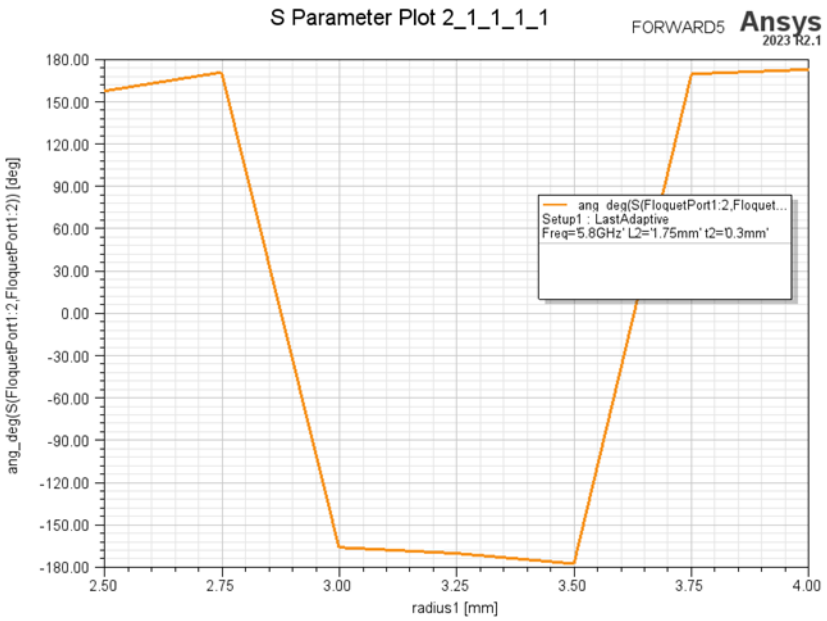

Figure 14. Phase difference with different RF chokes radius

In order to obtain a optimal radius for RF chokes, we consider the radius as a variable and sweep it for simulation as shown in Figure 13 and 14. Eventually 4.00mm and 60 degrees is chosen for the radius and angle of the RF choke since as shown in figure 13 and 14, a 4.00mm radius has the lowest magnitude loss in forward bias mode, and the phase modulation is close to 180 degrees.

For the final complete simulation, all the components on unit cells are included and fixed.

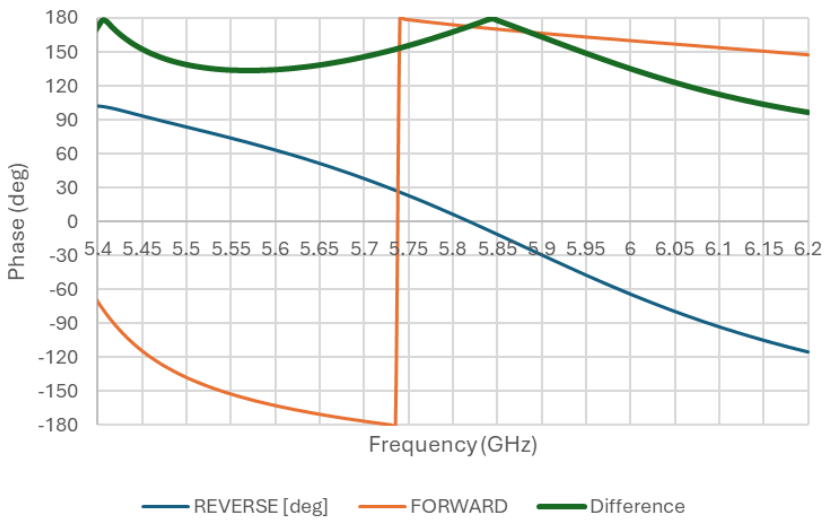

Figure 15. Phase modulation for final unit cell design

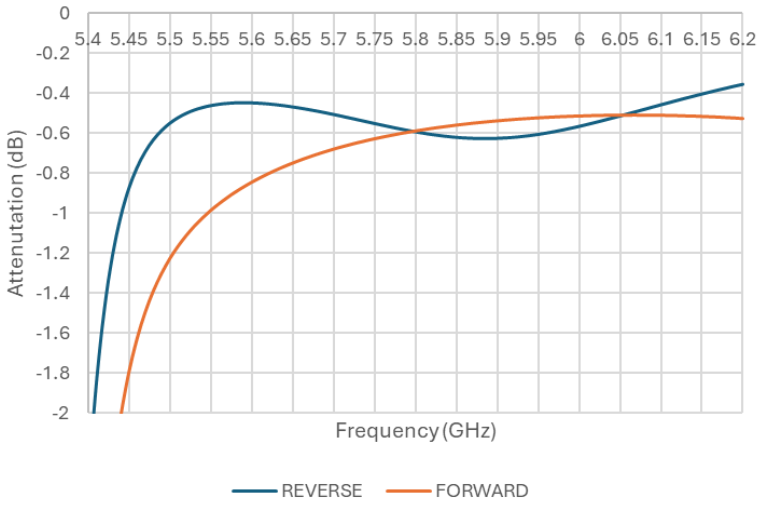

Figure 16. Magnitude attenuation (loss) for final design

As depicted in Fig. 15 and 16, the disparity in the reflected signal's magnitude remains minimal (< 1 dB) between the two states, while the phase difference is maintained at 180° at 5.85 GHz. The center resonant frequency is being shifted by a small amount due to the transmission lines and RF chokes. However, with an acceptable phase modulation range of 180° ± 20° between the states, the anticipated bandwidth is approximately 100 MHz, as illustrated in Fig. 15 and 16. Which means the RIS unit cell can still have an ideal performance for 5.8GHz, which meets our expectation and goal. It's worth noting that

the angle of incidence and the mutual coupling (finite array) will also influence the magnitude and phase response, ultimately determining the RIS's overall scanning capability and bandwidth performance.

5. Conclusion

In this study, we developed a proof-of-concept prototype for reconfigurable intelligent surfaces and assessed their potential benefits in real-world scenarios and practical applications. Specifically, we engineered and constructed a sub-6 GHz 160-element RIS prototype, featuring a planar single-layer reconfigurable reflectarray without vias, enabling scanning in both azimuth and elevation planes. Due to the straightforward geometry and the utilization of single-bit switches, the proposed design can be seamlessly adapted to higher frequencies such as mmWave and THz systems, employing RF PIN switches, transistor-based switches (e.g., CMOS-based), or tunable materials (e.g., graphene) [1].

This study has demonstrated that Reconfigurable Intelligent Surfaces (RISs) represent a promising technology for extending wireless coverage in scenarios characterized by strong occlusions, even when the RIS is situated in the far field of both the base station and the mobile user. Furthermore, RISs have the potential to operate at extremely low power levels, which is crucial for: i) promoting sustainable wireless communications, and ii) facilitating deployments in areas with limited or nonexistent access to power supplies. The current non-optimized diode and shift register consume less than 5 mW (including the biasing circuitry) for each unit cell. As an alternative to PIN diodes, transistor-based switches [20] offer promising prospects for RISs with extremely low power consumption.

References

[1] G. C. Trichopoulos et al., "Design and Evaluation of Reconfigurable Intelligent Surfaces in Real-World Environment," in IEEE Open Journal of the Communications Society, vol. 3, pp. 462-474, 2022, doi: 10.1109/OJCOMS.2022.3158310.

[2] H. Zhang, L. Song, Z. Han and H. V. Poor, "Spatial Equalization Before Reception: Reconfigurable Intelligent Surfaces for Multi-Path Mitigation," ICASSP 2021 - 2021 IEEE International Conference on Acoustics, Speech and Signal Processing (ICASSP), Toronto, ON, Canada, 2021, pp. 8062-8066, doi: 10.1109/ICASSP39728.2021.9414612.

[3] P. Zheng, J. Ding, D. Fei, J. Zhang, B. Ai, X. Li, S. Jin, T. Cui, Field trial measurement and channel modeling for reconfigurable intelligent surface, Digital Communications and Networks (2022), doi: https://doi.org/10.1016/j.dcan.2022.10.001.

[4] A. Araghi et al., "Reconfigurable Intelligent Surface (RIS) in the Sub-6 GHz Band: Design, Implementation, and Real-World Demonstration," in IEEE Access, vol. 10, pp. 2646-2655, 2022, doi: 10.1109/ACCESS.2022.3140278.

[5] X. Pei et al., “RIS-Aided Wireless Communications: Prototyping, Adaptive Beamforming, and Indoor/Outdoor Field Trials,” vol. 69, no. 12, pp. 8627–8640, Dec. 2021, doi: https://doi.org/10.1109/tcomm.2021.3116151.

[6] S. Lim, W. C. Choi, Y. J. Yoon and K. S. Ryu, "Isolation technique using the A/4 Stub RF Choke for the mobile MIMO system," 2015 International Workshop on Antenna Technology (iWAT), Seoul, Korea (South), 2015, pp. 164-167, doi: 10.1109/IWAT.2015.7365362.

[7] E. Cišija, A. M. Ahmed, A. Sezgin, and H. Wymeersch, “RIS-aided ˇ mmWave MIMO radar system for adaptive multi-target localization,” in Proc. IEEE Stat. Signal Process. Workshop (SSP), Rio de Janeiro, Brazil, 2021, pp. 196–200.

[8] N. Yu et al., “Light propagation with phase discontinuities: Generalized laws of reflection and refraction,” Science, vol. 334, no. 6054, pp. 333–337, Oct. 2011. [Online]. Available: https://science.sciencemag.org/content/334/6054/333

[9] X. Pei et al., “RIS-aided wireless communications: Prototyping, adaptive beamforming, and indoor/outdoor field trials,” Feb. 2021, arXiv:2103.00534.

[10] H. Yang et al., “A study of phase quantization effects for reconfigurable reflectarray antennas,” IEEE Antennas Wireless Propag. Lett., vol. 16, pp. 302–305, 2017.

[11] S. V. Hum, M. Okoniewski, and R. J. Davies, “Modeling and design of electronically tunable reflectarrays,” IEEE Trans. Antennas Propag., vol. 55, no. 8, pp. 2200–2210, Aug. 2007.

[12] “Basic OFDM Tutorial.” Basic OFDM Tutorial - GNU Radio, wiki.gnuradio.org/index.php/Basic_OFDM_Tutorial. Accessed 25 Sept. 2023

[13] T. M. Schmidl and D. C. Cox, "Robust frequency and timing synchronization for OFDM," in IEEE Transactions on Communications, vol. 45, no. 12, pp. 1613-1621, Dec. 1997, doi: 10.1109/26.650240.

[14] “Header/Payload Demux.” Header/Payload Demux - GNU Radio, wiki.gnuradio.org/index.php/Header/Payload_Demux. Accessed 25 Sept. 2023.

[15] “OFDM Carrier Allocator.” OFDM Carrier Allocator - GNU Radio, wiki.gnuradio.org/index.php/OFDM_Carrier_Allocator. Accessed 25 Sept. 2023.

[16] “OFDM Channel Estimation.” OFDM Channel Estimation - GNU Radio, wiki.gnuradio.org/index.php/OFDM_Channel_Estimation. Accessed 25 Sept. 2023.

[17] “OFDM Frame Equalizer.” OFDM Frame Equalizer - GNU Radio, wiki.gnuradio.org/index.php/OFDM_Frame_Equalizer. Accessed 25 Sept. 2023.

[18] “OFDM Serializer.” OFDM Serializer - GNU Radio, wiki.gnuradio.org/index.php/OFDM_Serializer. Accessed 25 Sept. 2023.

[19] “Schmidl & Cox Ofdm Synch.” Schmidl & Cox OFDM Synch. - GNU Radio, wiki.gnuradio.org/index.php/Schmidl_%26_Cox_OFDM_synch. Accessed 25 Sept. 2023.

[20] S. Venkatesh, X. Lu, H. Saeidi, and K. Sengupta, "A high speed programmable and scalable terahertz holographic metasurface based on tiled CMOS chips," Nat. Electron., vol. 3, no. 12, pp. 785–793, Dec. 2020. [Online]. Available: http://www.nature.com/articles/s41928-020-00497-2

[21] Q. Wu, S. Zhang, B. Zheng, C. You and R. Zhang, "Intelligent Reflecting Surface-Aided Wireless Communications: A Tutorial," in IEEE Transactions on Communications, vol. 69, no. 5, pp. 3313-3351, May 2021, doi: 10.1109/TCOMM.2021.3051897.

[22] Y. Ai, F. A. P. deFigueiredo, L. Kong, M. Cheffena, S. Chatzinotas and B. Ottersten, "Secure Vehicular Communications Through Reconfigurable Intelligent Surfaces," in IEEE Transactions on Vehicular Technology, vol. 70, no. 7, pp. 7272-7276, July 2021, doi: 10.1109/TVT.2021.3088441.

[23] A. U. Makarfi, K. M. Rabie, O. Kaiwartya, X. Li and R. Kharel, "Physical Layer Security in Vehicular Networks with Reconfigurable Intelligent Surfaces," 2020 IEEE 91st Vehicular Technology Conference (VTC2020-Spring), Antwerp, Belgium, 2020, pp. 1-6, doi: 10.1109/VTC2020-Spring48590.2020.9128438.

[24] C. Huang, A. Zappone, G. C. Alexandropoulos, M. Debbah and C. Yuen, "Reconfigurable Intelligent Surfaces for Energy Efficiency in Wireless Communication," in IEEE Transactions on Wireless Communications, vol. 18, no. 8, pp. 4157-4170, Aug. 2019, doi: 10.1109/TWC.2019.2922609.

[25] E. Basar, M. Di Renzo, J. De Rosny, M. Debbah, M. -S. Alouini and R. Zhang, "Wireless Communications Through Reconfigurable Intelligent Surfaces," in IEEE Access, vol. 7, pp. 116753-116773, 2019, doi: 10.1109/ACCESS.2019.2935192.

[26] M. H. Mahmud, M. M. Hossain, A. A. Khan, S. Ahmed, M. A. Mahmud and M. H. Islam, "Performance Analysis of OFDM, W-OFDM and F-OFDM Under Rayleigh Fading Channel for 5G Wireless Communication," 2020 3rd International Conference on Intelligent Sustainable Systems (ICISS), Thoothukudi, India, 2020, pp. 1172-1177, doi: 10.1109/ICISS49785.2020.9316134.

Appendix A: GNURadio QPSK OFDM System

GNURadio has the embedded operation and modulation modules for OFDM algorithm. The embedded modules integrate various of functions for you to customize and adjust your OFDM system. What's more, GNURadio also allows users to create their own function blocks by using C++ or Python. In this project, we are focusing on using embedded function modules to construct the OFDM system.

A.1 OFDM Tx:

In general, transmitters in communication systems work as a preliminary signal processing unit which takes the input digital data and formats them into message analog transmittable wave. In order to do that, transmitters must have the following functionalities:

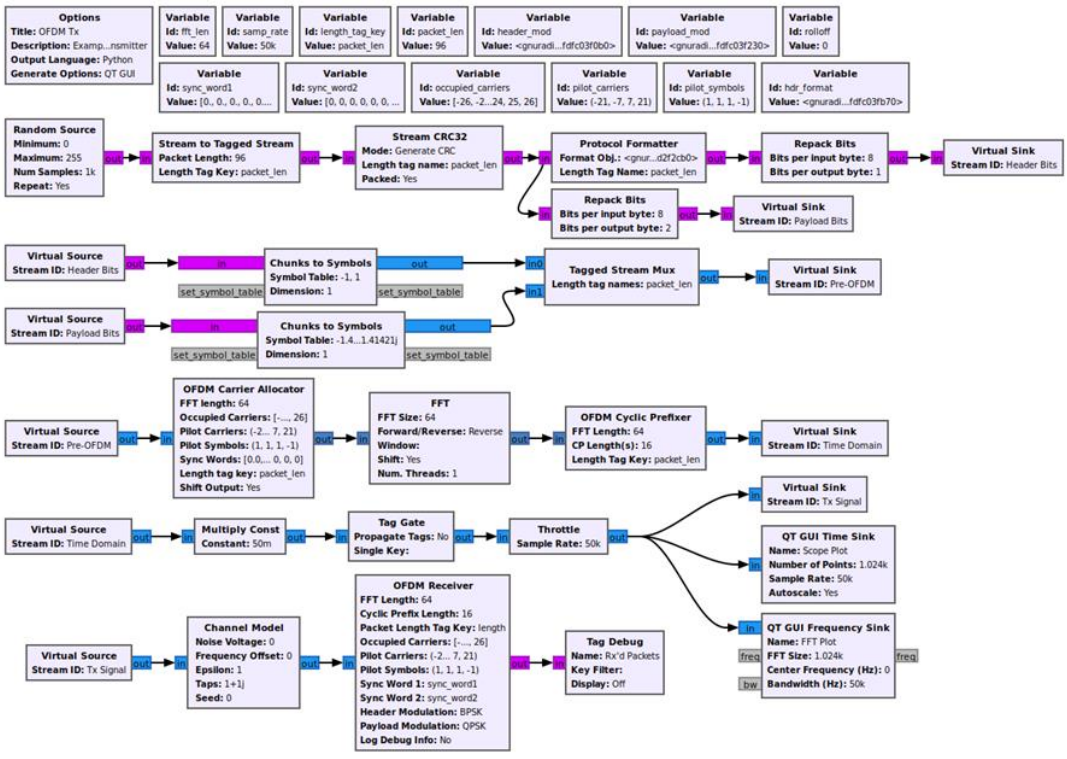

Figure 17. OFDM Transmitter Block Diagram

1. Symbol encoding (Modulation): Modulation is the process of varying a carrier signal's properties, such as its amplitude, frequency, or phase, to encode information or data onto it for transmission. By using different types of modulation, we can maximize the communication

efficiency and antenna efficiency. Moreover, Modulation can also be used to improve a signal's resilience to noise and interference. By spreading the signal's energy over a wider frequency range (as in spread spectrum modulation techniques), it becomes more robust against narrowband interference or jamming.

In this OFDM design, BPSK and QPSK were used for header and payload bits encoding. *Chunks to Symbol* blocks are used for symbol mapping in this design, it takes the input header and payload bits and maps them separately. After encoding, header and payload were combined by *Tagged Stream Mux*.

2. Guard bin insertion and Inverse Fast Fourier Transform: Since OFDM systems will divide the frequency bandwidth into sub-carriers and transmit the symbol in frequency domain, the subcarriers are orthogonal to each other but should not be located close to channels, therefore, we need to insert guard bin and DC bin at the side and middle of the channels. There should be no data bits inside the guard bins and DC bins.

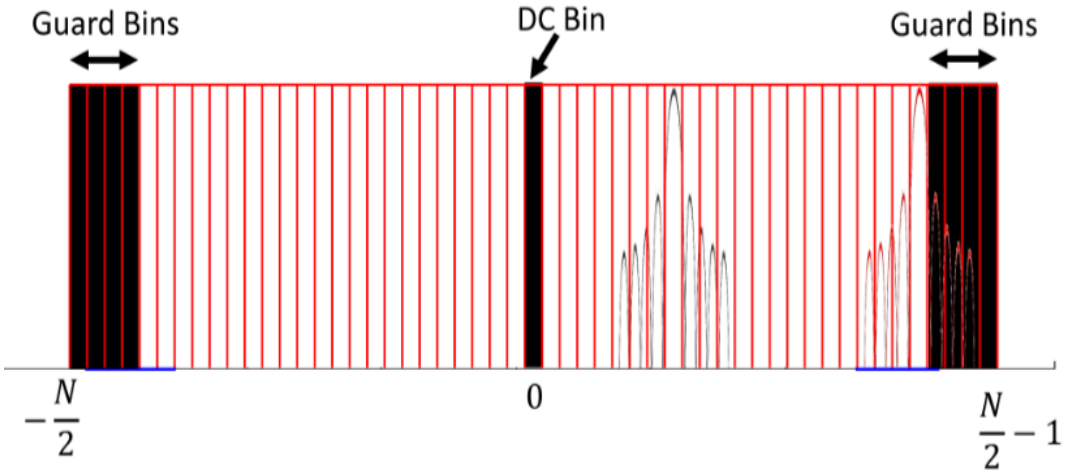

Figure 18. How DC guard bins are used

In GNURadio, there is an embedded function that could be used for allocating data into each sub-carrier and inserting guard bin and DC bin, which is *OFDM Carrier Allocator*. It allows users to define the FFT length, guard bin locations, and carrier locations, and then it will

automatically assign the data message into the corresponding carrier. *OFDM Carreri Allocator* can directly be connected to *FFT* block, which is used for reverse FFT (IFFT) to transform the frequency domain symbols to time domain for USRP.

3. Cyclic Prefix: A cyclic prefix is a redundant segment of the transmitted signal, consisting of a copy of the end of the symbol appended to the beginning. The cyclic prefix is inserted before each symbol in the data stream. Its length is typically chosen to be longer than the expected delay spread of the channel, ensuring that delayed versions of the signal do not interfere with the current symbol.

A.2 OFDM Rx:

An OFDM receiver is responsible for demodulating and decoding OFDM signals. The received OFDM signal is captured by an antenna and processed by the receiver's front-end circuitry, which includes amplification and filtering.

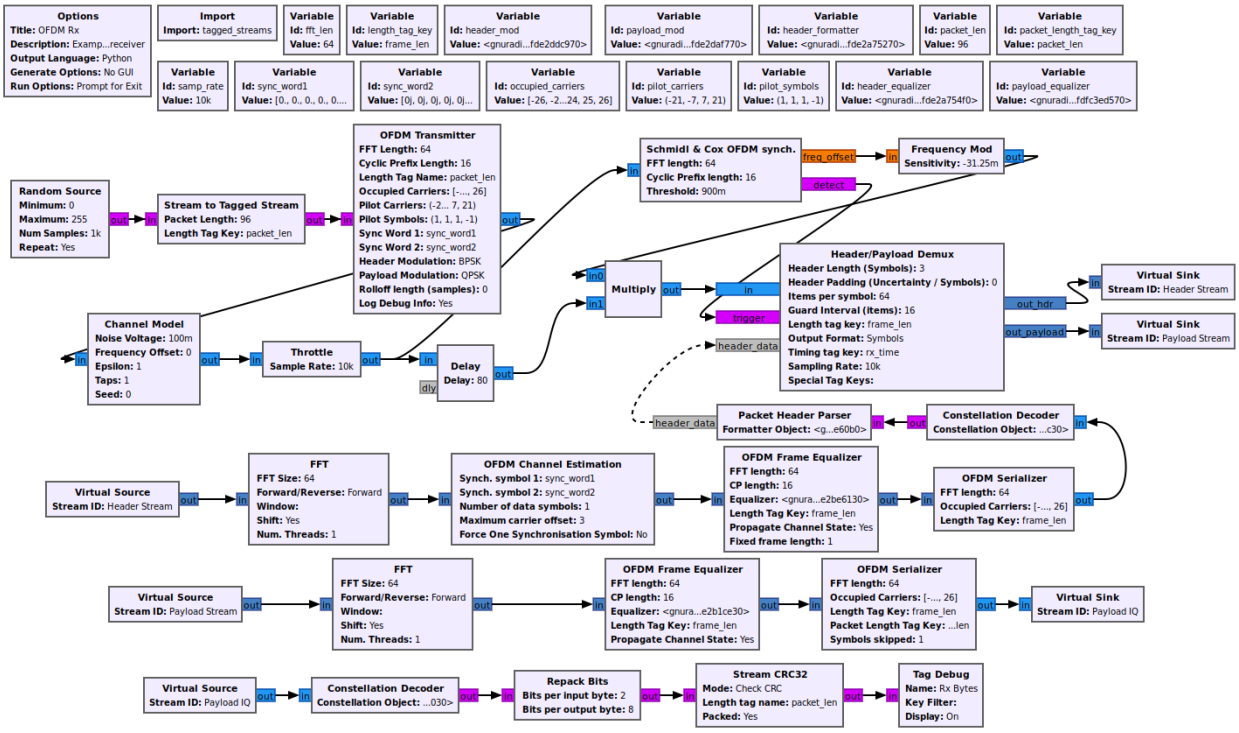

Figure 19. OFDM Rx

Here's an overview of the components and operations typically found in an OFDM receiver:

1. Frequency Offset Correction: During the transmission process, frequency offset could be added toward the message wave. Frequency offset could potentially by communication hardware systems. It could be from the clock mismatch inside the hardware or the signal glitches in FPGA. Frequency offset misaligns the received signal pulses and changes the phase of the received message wave, which will prevent us from decoding the message correctly.

   In order to eliminate the effect from frequency offset, we implemented the frequency offset correction function to correct the phase offset for received signal waves. In this OFDM design, we used Fine and Coarse Frequency Offset Correction to fully eliminate the frequency offset. Fine Frequency Offset Correction is used for compensating the offset that is smaller than one sub-carrier spacing.

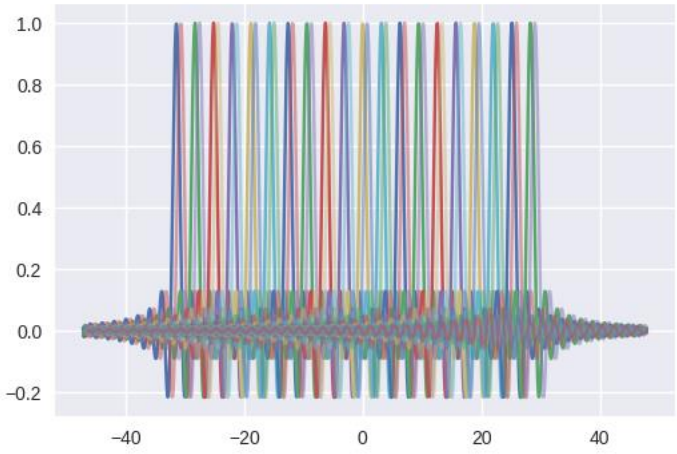

Figure 20. Small Frequency Offset

Schmidl & Cox OFDM synch is used for fine frequency correction. It is a rapid and robust synchronization of OFDM signals. It utilizes the training sequence and averaging all subchannels, which will provide accurate estimations for carrier frequency offset.

Coarse Frequency Offset Correction is used for compensating the frequency offset that is larger than one sub-carrier spacing.

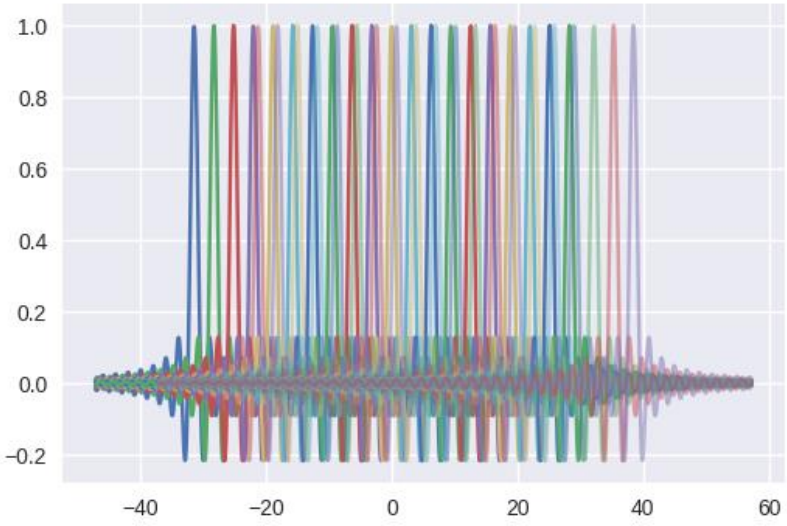

Figure 21. Large Frequency Offset

In this design, we will use the embedded function *OFDM Frame Equalizer* for coarse frequency correction. Unlike fine frequency compensation, *OFDM Frame Equalizer* does not use training sequences to provide the estimations. Instead, it utilizes the tag from each packet to align the OFDM signals.

2. Frame Synchronization: Frame synchronization is a crucial process in digital communication systems. It ensures that the receiver correctly aligns with the transmitted data frames or packets, allowing for the accurate demodulation and decoding of the information. Frame synchronization is particularly important in scenarios where data is divided into discrete frames or packets. In our design, we implemented *Header/Payload Demux* to synchronize the frame and separate the header messages and payloads. This embedded function block will detect the trigger, which is the tag for header, and this trigger indicates the start of headers. Once the trigger is detected, it will keep reading the symbols until the number of symbols being read is equal to the length of the headers. The next symbol will be the start of the payload, and the payload will be copied to output 1. Therefore, we will receive header and payload separately at the output of this function. Moreover, *Header/Payload Demux* will remove the cyclic prefix and return the symbols.
3. Channel Estimation: Orthogonal Frequency Division Multiplexing (OFDM) channel estimation is a crucial component of OFDM-based communication systems. It involves estimating the frequency response characteristics of the communication channel to compensate for its effects, such as attenuation and frequency-selective fading. Accurate channel estimation is essential for demodulation and decoding of transmitted data.

   OFDM Channel Estimation is implemented for channel estimation and correction. The embedded function will take OFDM header symbols in frequency domain, therefore we need to

perform Fast Fourier Transform (FFT) for header first. The first one (or two) symbols are expected to be synchronization symbols, which are used to estimate the initial equalizer taps. The following n data symbols are passed through unmodified. Estimated channel coefficient will be passed to *Frame Equalizer*, which will be used to correct the symbols.

4. Remove Null Tones: At the transmitter side, Null Tones and DC bin were inserted in order to enhance the performance of the OFDM system. In order to retrieve the correct message, Null Tones and DC bin must be removed before decoding. We implement *OFDM Serializer* to remove the Null Tones and DC bins in sub-carriers. It will take the location of the Null Tones and DC bins and remove the corresponding sub-carrier.
5. Symbol Decoding: The final step for the receiver will be decoding. Since payload was modulated into QPSK symbols, a QPSK decoder is needed to demodulate the received symbol to original binary data bits.

A.3 GNURadio OFDM System Performance

For OFDM data transmission, we initially tested the implemented GNU Radio OFDM system by repetitively transmitting simple text messages using the USRP X310 with two dipole antennas in 5.8 GHz frequency band.

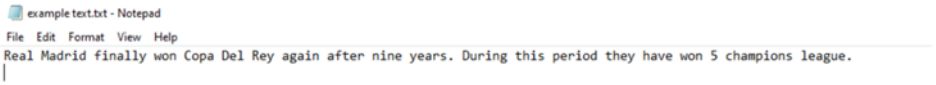

Figure 22. Example text message for transmitting

```
Real Madrid finally won Copa Del Rey again after nine years. During this period they have won 5 champions league.
Real Madrid finally won Copa Del Rey again after nine years. During this period they have won 5 champions league.
Real Madrid finally won Copa Del Rey again after nine years. During this period they have won 5 champions league.
Real Madrid finally won Copa Del Rey again after nine years. During this period they have won 5 champions league.
Real Madrid finally won Copa Del Rey again after nine years. During this period they have won 5 champions league.
Real Madrid finally won Copa Del Rey again after nine years. During this period they have won 5 champions league.
Real Madrid finally won Copa Del Rey again after nine years. During this period they have won 5 champions league.
Real Madrid finally won Copa Del Rey again after nine years. During this period they have won 5 champions league.
Real Madrid finally won Copa Del Rey again after nine years. During this period they have won 5 champions league.
Real Madrid finally won Copa Del Rey again after nine years. During this period they have won 5 champions league.
Real Madrid finally won Copa Del Rey again after nine years. During this period they have won 5 champions league.
Real Madrid finally won Copa Del Rey again after nine years. During this period they have won 5 champions league.
Real Madrid finally won Copa Del Rey again after nine years. During this period they have won 5 champions league.
Real Madrid finally won Copa Del Rey again after nine years. During this period they have won 5 champions league.
Real Madrid finally won Copa Del Rey again after nine years. During this period they have won 5 champions league.
Real Madrid finally won Copa Del Rey again after nine years. During this period they have won 5 champions league.
Real Madrid finally won Copa Del Rey again after nine years. During this period they have won 5 champions league.
Real Madrid finally won Copa Del Rey again after nine years. During this period they have won 5 champions league.
Real Madrid finally won Copa Del Rey again after nine years. During this period they have won 5 champions league.
Real Madrid finally won Copa Del Rey again after nine years. During this period they have won 5 champions league.
Real Madrid finally won Copa Del Rey again after nine years. During this period they have won 5 champions league.
Real Madrid finally won Copa Del Rey again after nine years. During this period they have won 5 champions league.
Real Madrid finally won Copa Del Rey again after nine years. During this period they have won 5 champions league.
Real Madrid finally won Copa Del Rey again after nine years. During this period they have won 5 champions league.
Real Madrid finally won Copa Del Rey again after nine years. During this period they have won 5 champions league.
Real Madrid finally won Copa Del Rey again after nine years. During this period they have won 5 champions league.
Real Madrid finally won Copa Del Rey again after nine years. During this period they have won 5 champions league.
Real Madrid finally won Copa Del Rey again after nine years. During this period they have won 5 champions league.
Real Madrid finally won Copa Del Rey again after nine years. During this period they have won 5 champions league.
Real Madrid finally won Copa Del Rey again after nine years. During this period they have won 5 champions league.
Real Madrid finally won Copa Del Rey again after nine years. During this period they have won 5 champions league.
Real Madrid finally won Copa Del Rey again after nine years. During this period they have won 5 champions league.
Real Madrid finally won Copa Del Rey again after nine years. During this period they have won 5 champions league.
Real Madrid finally won Copa Del Rey again after nine years. During this period they have won 5 champions league.
Real Madrid finally won Copa Del Rey again after nine years. During this period they have won 5 champions league.
```

Figure 23. Received text messages

As shown in figure 22 and 23, we were able to successfully receive and decode the message when transmitting it at 5.8 GHz with a sampling rate of 1 MHz.

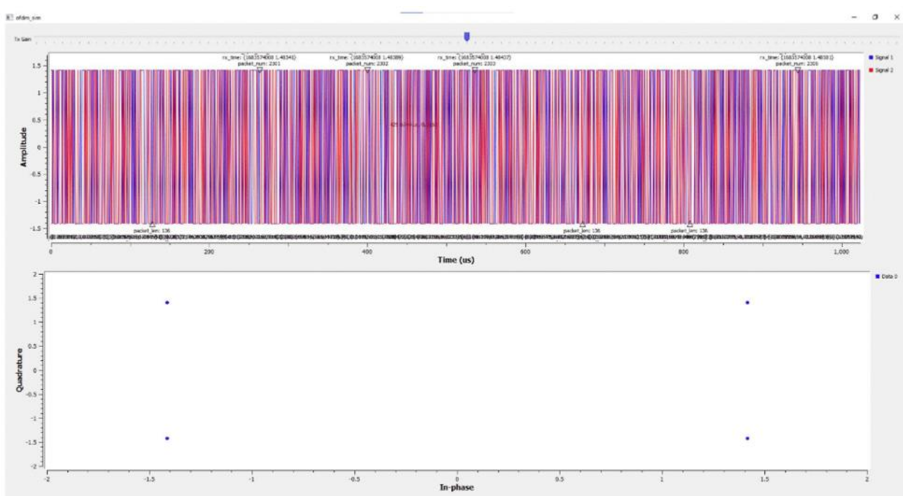

Figure 24. Received signals with symbol constellation diagram

Furthermore, the performance of our OFDM system can be visualized using a constellation diagram. As shown in Figure 24, the constellation diagram represents the received symbols after channel equalization, CFO correction, and FFT processing, displaying a QPSK modulation symbol diagram.